Emergent dynamics of a three-node regulatory network explain phenotypic switching and heterogeneity: a case study of Th1/Th2/Th17 cell differentiation

Atchuta Srinivas Duddu[a], Sauma Suvra Majumdar[b], Sarthak Sahoo[a], Siddharth Jhunjhunwala[a], and Mohit Kumar Jolly[a,*]

[a]Centre for BioSystems Science and Engineering, Indian Institute of Science, Bangalore 560012, India; [b]Department of Biotechnology, National Institute of Technology, Durgapur 713216, India

ABSTRACT **Naïve helper (CD4+) T-cells can differentiate into distinct functional subsets including Th1, Th2, and Th17 phenotypes. Each of these phenotypes has a "master regulator"—T-bet (Th1), GATA3 (Th2), and RORγT (Th17)—that inhibits the other two master regulators. Such mutual repression among them at a transcriptional level can enable multistability, giving rise to six experimentally observed phenotype, Th1, Th2, Th17, hybrid Th/Th2, hybrid Th2/Th17, and hybrid Th1/Th17. However, the dynamics of switching among these phenotypes, particularly in the case of epigenetic influence, remain unclear. Here through mathematical modeling, we investigated the coupled transcription-epigenetic dynamics in a three-node mutually repressing network to elucidate how epigenetic changes mediated by any master regulator can influence the transition rates among different cellular phenotypes. We show that the degree of plasticity exhibited by one phenotype depends on relative strength and duration of mutual epigenetic repression mediated among the master regulators in a three-node network. Further, our model predictions can offer putative mechanisms underlying relatively higher plasticity of Th17 phenotype as observed in vitro and in vivo. Together, our modeling framework characterizes phenotypic plasticity and heterogeneity as an outcome of emergent dynamics of a three-node regulatory network, such as the one mediated by T-bet/GATA3/RORγT.**

Monitoring Editor
Alex Mogilner
New York University

Received: Nov 3, 2021
Revised: Mar 14, 2022
Accepted: Mar 22, 2022

This article was published online ahead of print in MBoC in Press (http://www.molbiolcell.org/cgi/doi/10.1091/mbc.E21-10-0521) on March 30, 2022.

Conflict of interest: the authors declare no conflict of interest.

Author contributors: M.K.J. conceived and supervised research; A.S.D., S.S.M. and S.S. performed research; all authors contributed to the data analysis and interpretation and in preparing the paper.

Data availability: all parameter sets used here are given in Supplemental Table S1. All codes used are given at the following GitHub repository: https://github.com/csbBSSE/Toggle-Triad-Epigenetics.

*Address correspondence to: Mohit Kumar Jolly (mkjolly@iisc.ac.in).

Abbreviations used: HDACs, histone de-acetylases; ssGSEA, single sample gene set enrichment analysis; Th, T-helper; TF, transcription factor.

INTRODUCTION

Differentiation of naïve CD4+ T-cells into diverse T-helper (Th) cells facilitates versatile and adaptable immune responses to different challenges and serves as a powerful model system to investigate cell-fate decision making (Evans and Jenner, 2013). Different Th cells—Th1, Th2, and Th17 among others—have distinct cytokine and functional profiles. Th1 cells mainly produce IFNγ, and mediate host defense against intracellular bacteria and viruses, while Th2 cells produce IL-4 and are implicated in allergic immune responses. Th17 cells secrete IL-17A, IL-17F, and GM-CSF and act against bacterial and fungal pathogens such as *Mycobacterium* (Kaiko *et al*., 2008; Stadhouders *et al*., 2018). Earlier thought to be mutually exclusive and (terminally) stable phenotypes, recent single-cell evidence has revealed the heterogeneity and plasticity of Th cell

subsets. For instance, hybrid Th1/Th2, Th2/Th17, and Th1/Th17 phenotypes have been observed at a single-cell level in vitro and in vivo (Peine *et al.*, 2013; Chatterjee *et al.*, 2018; Xhangholi *et al.*, 2019; Tortola *et al.*, 2020). Moreover, in vitro restimulation can drive switching among multiple phenotypes Th1, Th2, and Th17 and the corresponding hybrid ones (Curtis *et al.*, 2010; Evans and Jenner, 2013; Tortola *et al.*, 2020; Cerboni *et al.*, 2021). However, a dynamical characterization of phenotypic switching among these Th cell subpopulations has not been performed.

T-bet, GATA3, and RORγT have been proposed as the "master regulators" of Th1, Th2, and Th17 cells, respectively. They can mutually repress each other and self-activate directly or indirectly, thus driving CD4+ naïve cell differentiation into diverse Th subsets (Fang and Zhu, 2017). Such mutual repression is a hallmark of "sibling" cell-fates in many systems, such as for PU.1/GATA1 in the case of common myeloid progenitor differentiating to a myeloid or erythroid fate (Zhou and Huang, 2011), or ZEB1/ GRHL2 for epithelial-mesenchymal transition (Hari *et al.*, 2020). Similarly to PU.1/GATA1 and ZEB1/ GRHL2, the T-bet/GATA3/RORγT regulatory network can be multistable, enabling the coexistence of different phenotypes and switching among them—Th1 (high T-bet, low GATA3, low RORγT), Th2 (low T-bet, high GATA3, low RORγT), Th17 (low T-bet, low GATA3, high RORγT), hybrid Th1/Th2 (high T-bet, high GATA3, low RORγT), hybrid Th2/Th17 (low T-bet, high GATA3, high RORγT), and hybrid Th1/Th17 (high T-bet, low GATA3, high RORγT). Intriguingly, self-activation of master regulators can enrich for hybrid phenotypes (Duddu *et al.*, 2020). However, a comprehensive analysis of the interplay among factors influencing the rates of transition among these phenotypes remains to be done.

Epigenetic changes, including modifications of histones and DNA methylation status, can control the rate of phenotypic switching by influencing the access of master regulators to their genome-wide targets. Thus cell-specific chromatin landscape and "histone code" can form stable epigenetic marks at various gene loci, thus governing the commitment, heritability, and plasticity of various cell-fates (Chang and Aune, 2007; Miyamoto *et al.*, 2015; Suelves *et al.*, 2016). Early biochemical evidence for the importance of epigenetic processes in T-cell differentiation came from studies showing that treatment of T-cells with inhibitors of histone de-acetylases (HDACs) or DNA methylation led to the production of IL-2 and IFNγ by cells that could not previously produce them (Wilson *et al.*, 2009). Further, T-bet, GATA3, and RORγT have been shown to control chromatin accessibility required for T-cell differentiation into different lineages/phenotypes (Sanders, 2006; Hirahara *et al.*, 2011). Interestingly, such influence was shown to be at least partly independent of signals from cytokine receptors/signaling, suggesting many parallel paths that these master regulators can take to suppress other lineages and to promote their own (Josefowicz, 2013; Lee *et al.*, 2020). Epigenetic changes such as chromatin remodeling are crucial not only for CD4+ T-cell differentiation but also for lineage stability (Renaude *et al.*, 2021). For instance, in Th2 cells, repressive histone marks H3K27me3 and H3K9me3 are deposited on Th1-associated genes, thus forming heterochromatin at those specific promoters and establishing transcriptional silencing. Such epigenetic changes drive lineage stability and often need to be "erased" for reprogramming.

Once differentiated, Th subsets are often reprogrammed to other ones during injury response and resolution (Tortola *et al.*, 2020). The stronger the lineage stability mechanisms in a cell the less reprogrammable it can become. While mutual antagonism at transcriptional and epigenetic levels enable the establishment of a cell-state and have been witnessed in other cellular decision-making contexts (Tripathi *et al.*, 2020; Serresi *et al.*, 2021), they can differently control the reprogramming rates. For example, in various instances, "epigenetically locked" cells can be difficult to reprogram (Nashun *et al.*, 2015; Baumann *et al.*, 2019; Eichelberger *et al.*, 2020). Despite such wealth of molecular and functional data for T-cell differentiation, we still lack a quantitative systems-level investigation of how the rates of phenotypic switching among Th1, Th2, and Th17 depend on the epigenetic influences mediated by T-bet, GATA3, and RORγT on each other.

Here we build on our previous study that showed that a mutually repressing three-node system enables three predominant states driven by each node, and that switching between these states was possible. However, the dynamics of switching and longevity (mean residence times) of these phenotypes, especially in cases where epigenetic control exists, remained unexplored. While Th cells are known to undergo similar switching, experimental data regarding the dynamics of the switches are scarce and the experiments are difficult to perform. Thus we have used a mathematical modeling approach to address the questions of emergent dynamics of a three-node system repressing each other at both transcriptional and epigenetic levels. Our simulations reveal that the rate of switching among phenotypes and the consequent changes in population distribution of cellular phenotypes are a function of the relative strength as well as duration corresponding to epigenetic repression mediated by the three master regulators on one another. The stronger the incoming epigenetic repression for a given master regulator the higher the probability of switching out of the corresponding phenotype. These results unravel a potential design principle of T-cell differentiation at individual cell and population levels.

RESULTS

Transcriptional dynamics of Th1, Th2, and Th17 induction and corresponding phenotypic plasticity

To assess the transcriptional dynamics of T-cell differentiation, we quantified the extent of changes in Th1, Th2, and Th17 signature gene-sets under diverse experimental conditions using publicly available datasets. First, we analyzed a RNA-seq dataset (GSE71645) in which naïve T-cells were cultured for 72 h either in a Th1-inducing medium (IL-12 treatment) or in a Th2-inducing medium (IL-4 treatment) (Kanduri *et al.*, 2015) and projected the samples on a two-dimensional plane of Th1 and Th2 ssGSEA (single-sample Gene Set Enrichment Analysis) scores (Subramanian *et al.*, 2005) (Figure 1Ai). We observed that cells treated with IL-12 showed a significant enrichment in Th1 signature while IL-4 treated cells showed an enrichment in Th2 signature (Figure 1Aii). Time-course microarray data collected for this experiment (GSE71566) demonstrated that relative enrichment of one of the two signatures (Th1 or Th2) can be seen as early as 3 d in culture (Figure 1B). Similar mutually opposing trends for Th1 and Th2 enrichments were also seen in another independent dataset (GSE62484) that contained populations of naïve T-cells, activated Th1, and activated Th2 cells (Figure 1C) (Hertweck *et al.*, 2016). Analysis of two other time-course transcriptomic datasets (GSE60678, GSE32959) reinforced our observations that a 3-d treatment of naïve CD4+ T with either a Th1- or a Th2-inducing medium began to show differential activation of Th1 or Th2 induction programs (Äijö *et al.*, 2012; Gustafsson *et al.*, 2015) and stabilized at later time points (Figure 1, D and E). These dynamics are reminiscent of many cell differentiation trajectories where a multipotent progenitor cell often coexpresses mutually opposing master regulators (and/or their targets) corresponding to two (or more) phenotypes. This multipotent state of a cell is destabilized under the impact of exogenous signals (cytokines, growth factors, etc.) that push

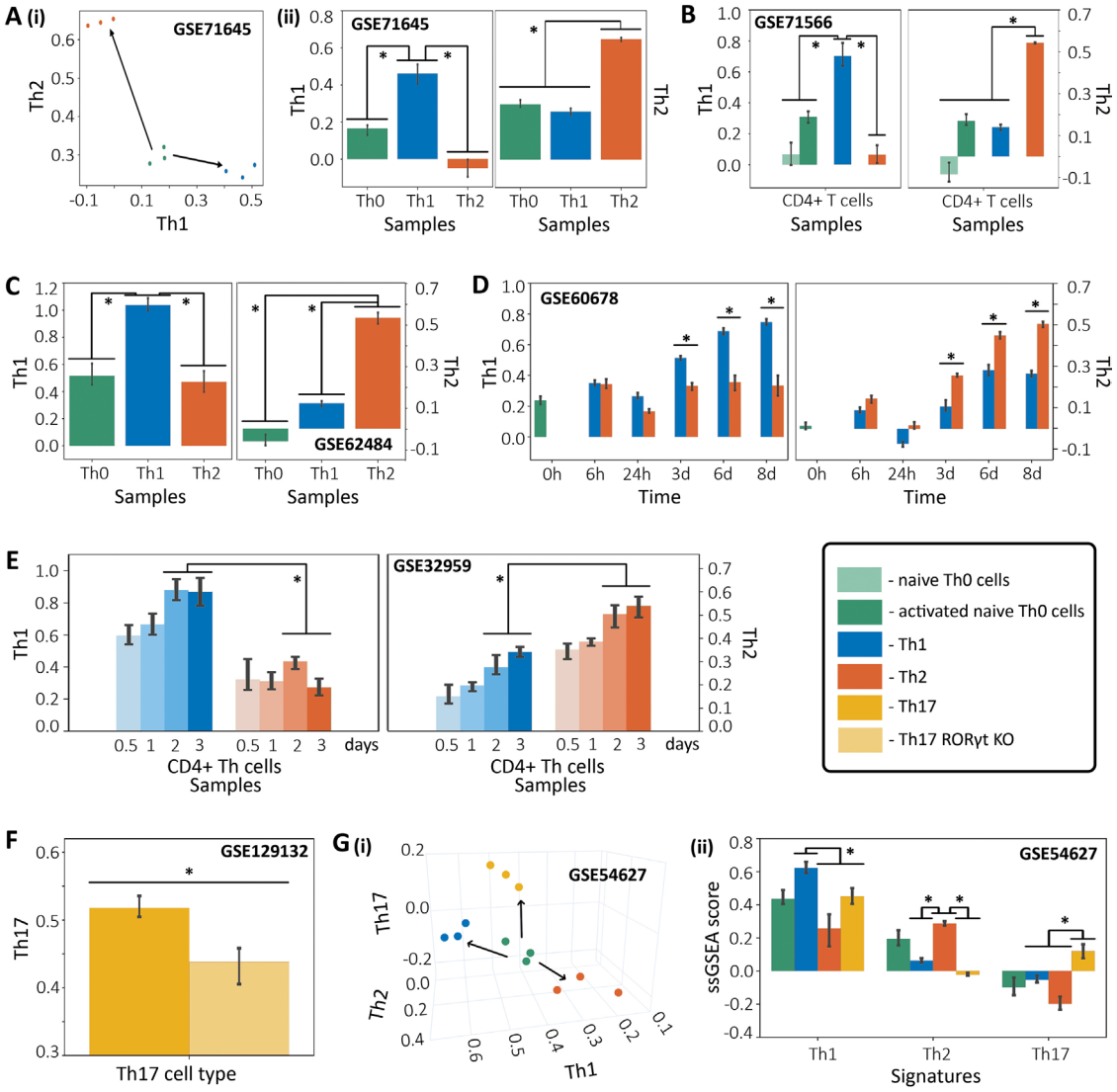

FIGURE 1: Transcriptomic analysis showing enrichment of Th1, Th2, and Th17 signatures specific to corresponding cell types. (A) (i) A 2D scatterplot showing T naïve, Th1, and Th2 cell types on the Th1-Th2 ssGSEA score plane. (ii) Quantification of differences in levels of Th1 and Th2 ssGSEA scores across T naïve, Th1, and Th2 cell types (GSE71645). (B) Quantification of differences in levels of Th1 and Th2 ssGSEA scores across T naïve, activated T naïve, induced Th1, and induced Th2 cell types (GSE71566). (C) Quantification of differences in levels of Th1 and Th2 ssGSEA scores across T naïve, activated Th1, and activated Th2 cell types (GSE62484). (D) Quantification of differences in levels of Th1 and Th2 ssGSEA scores across T naïve, Th1, and Th2 cell types over the time points 0 h, 6 h, 1 d, 3 d, 6 d, and 8 d (GSE60678). (E) Quantification of Th1 and TH2 ssGSEA scores for differentiating Th1 and Th2 cells over time points 0.5, 1, 2, and 3 d (GSE32959). (F) Quantification of differences in levels of Th17 ssGSEA scores across WT and RORγT knockout Th17 cells (GSE129132). (G) (i) A 3D scatterplot showing T naïve, Th1, Th2, and Th17 cell types on the Th1-Th2-Th17 ssGSEA score space in a nontreatment condition (control set at 0 h) and (ii) its corresponding (same condition) quantification of differences in the levels of Th1, Th2, and Th17 signatures (ssGSEA scores) (GSE54627). *Significantly different level of ssGSEA scores assessed by Students *t* test; p value < 0.05.

it toward an "attractor" corresponding to one of the differentiated states (Huang *et al.*, 2007; Bargaje *et al.*, 2017).

Next, we investigated transcriptomic signatures corresponding to Th17 differentiation and noticed that this signature captured the inhibition of Th17 differentiation when RORγT, a master regulator of Th17 cell state, was silenced in naïve CD4+ T-cells (Figure 1F) (GSE123192) (Lee *et al.*, 2020). Finally, we assessed how the three different cell types (Th1, Th2, Th17) are separated in a three-dimensional space of their ssGSEA scores (Figure 1G). We found that each of the cell types displayed significant enrichment of their corresponding signatures. Further, the T naïve cells are situated "intermediate" to the three cell-type signatures (Figure 1Gi), consistent with the undifferentiated state coexpressing markers of multiple phenotypes it can give rise to, as seen across biological contexts (Olsson *et al.*, 2016). We observed that Th1, Th2, and Th17 cells showed significant enrichment in their respective signatures while the signatures of the competing programs (for example, Th1 and Th2 programs during Th17 differentiation) were significantly suppressed (Figure 1Gii; GSE54627; Touzot *et al.*, 2014). Collectively, these results indicate the robust transcriptomic signatures associated with Th1, Th2, and Th17 induction during the trifurcation event during T-cell differentiation.

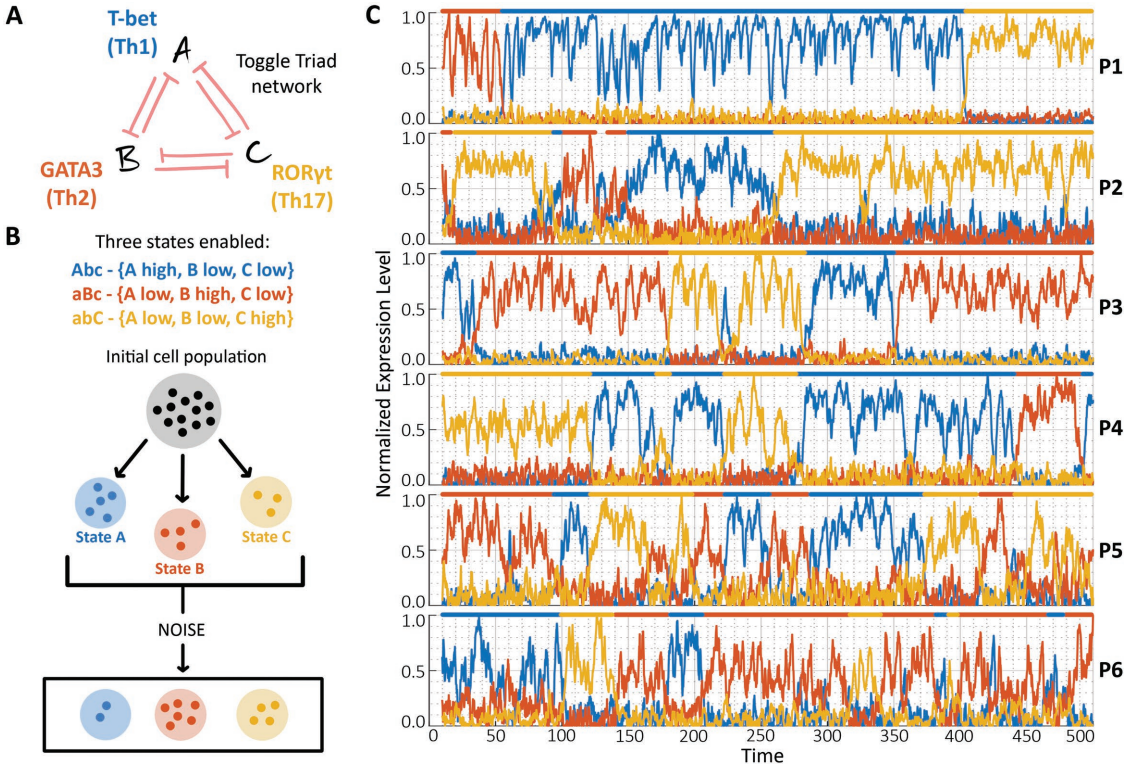

FIGURE 2: Phenotypic heterogeneity in Th cell population. (A) Toggle Triad network topology underlies the differentiation of naïve CD4+ T-cell into Th cells (Th1, Th2, and Th17). Each master regulator (T-bet, GATA3, and RORγT, respectively) mutually represses the other two. (B) The three states enabled by a toggle triad are listed along with notation used hereafter. A schematic representing a kinetic model with certain parameter set enabling a heterogenous population and noise enabling switching between the states. (C) Stochastic simulations of the network for different parameter sets (P1–P6 [Supplemental Table S1]) showing switching between the three states.

T-bet, GATA3, and RORγT—the proposed master regulators of Th1, Th2, and Th17, respectively—and their targets constitute the above-mentioned transcriptomic signatures associated with Th1, Th2, and Th17 differentiation (Radens *et al.*, 2020). They have been reported to mutually repress each other, thus pushing CD4+ naïve cells into diverse differentiation trajectories (Fang and Zhu, 2017), a trend robustly captured in transcriptomic datasets shown above. Thus a network of three mutually repressing regulators (A, B, and C) can serve as a model for CD4+ T-cell differentiation.

We have previously shown that such a "toggle triad" among A, B, and C (Figure 2A) can enable three predominant states (high A, low B, low C), (low A, high B, low C), and (low A, low B, high C; Figure 2B, represented by Abc, aBc, and abC correspondingly hereafter) (Duddu *et al.*, 2020). The states enabled by a toggle triad are reminiscent of emergent dynamics of a "toggle switch," a mutually inhibitory feedback loop between two master regulators that often enable two mutually exclusive states: (high A, low B) and (low A, high B) corresponding to a specific phenotype (Cherry and Adler, 2000; Gardner *et al.*, 2000; Graham *et al.*, 2010). A toggle switch explains the behavior of a progenitor cell differentiating into one of two cell fates, each fate driven majorly by a master transcription factor (TF). Similarly to phenotypic plasticity and heterogeneity observed in a toggle switch under the influence of noise (Gardner *et al.*, 2000; Ozbudak *et al.*, 2004), we would expect the three states enabled by a toggle triad to also be capable of switching among one another. To confirm this, we performed stochastic switching simulations for six different tristable parameter sets (P1–P6) that revealed possible switching among the three phenotypes: Abc (blue), aBc (red), and abC (yellow) (Figure 2C). The mean residence times in each state vary with the parameter set. However, across parameter sets, none of the states could be classified as transient/intermediate. For further characterization of the dynamical traits of the toggle triad, we mapped two phase diagrams for a representative parameter set with degradation or production rates of B and C (kB, kC; gB, gC) as the respective bifurcation parameters (Supplemental Figure S1).

Together, these results indicate that depending on the relative abundance of T-bet, GATA3, and RORγT, cells can exist in one or more of the three dominant phenotypes (Th1, Th2, and Th17) and can switch back and forth under the influence of stochastic fluctuations (biological noise). Such state-switching can induce and maintain phenotypic heterogeneity in a given Th cell population, with the relative frequencies of Th1, Th2, and Th17 dependent on relative levels of the master regulators (or equivalently, the concentration of different cytokines which can drive various cell-fates through their action on these master regulators).

Epigenetic repression driven by a master regulator can enrich for its corresponding phenotype in a heterogeneous population

Besides mutual repression at a transcriptional level, the three master regulators (T-bet, GATA3, and RORγT) can engage in epigenetic mutual repression as well (Mukasa *et al.*, 2010; Wei *et al.*, 2010; Zhu *et al.*, 2012; Sasaki *et al.*, 2013; Lee *et al.*, 2020). To incorporate epigenetic repression in our framework that captures transcriptional repression among these three master regulators, we utilized a phenomenological model approach (Miyamoto *et al.*, 2015) that introduces an epigenetic parameter (α) to quantify the threshold

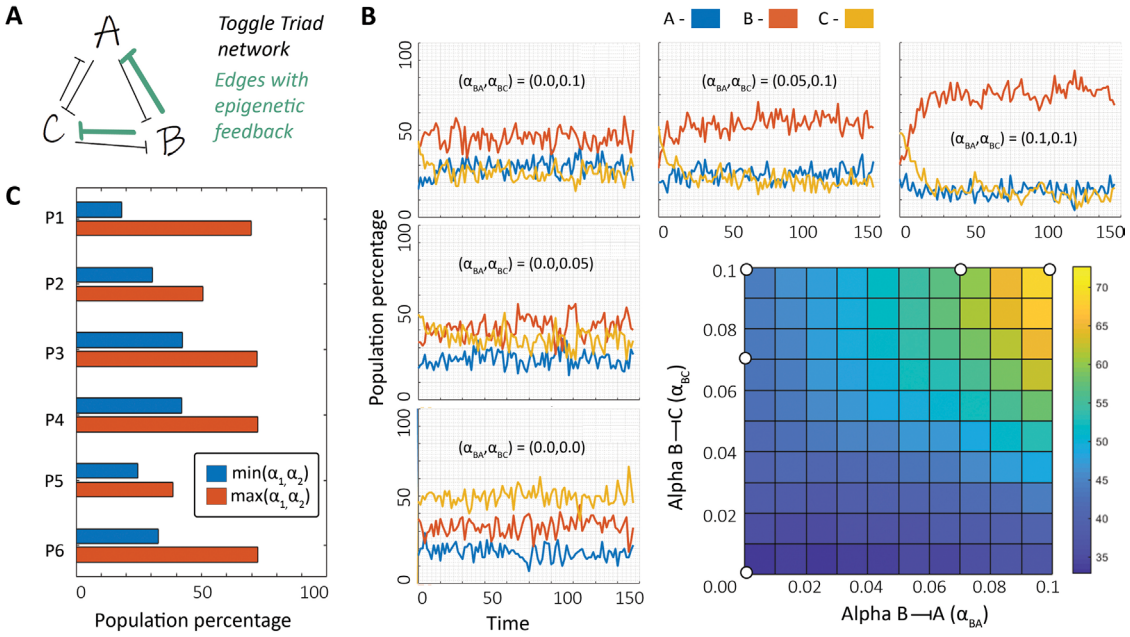

FIGURE 3: Epigenetic repression mediated by one node in toggle triad on the other two nodes. (A) Toggle triad network topology in which interactions incorporating epigenetic repression are marked in green. (B) Phase plot showing the population percentage of cells in state B (aBc) with bifurcation parameters as the α values corresponding to the epigenetic feedback of B -| A and B -| C, as well as dynamics of distribution of population percentage between states A, B, and C for certain pairs of α_{BA} and α_{BC} values. (C) Population percentage of the node from which interactions with epigenetic repression originate, with pair of α values at corresponding maximum and minimum for six parameter sets (P1–P6 given in SupplementalTable S1). Parameter set P6 used in B. Results for parameter sets P1–P5 shown in Supplemental Figures S2 and S3.

(half-maximal) levels corresponding to the influence of expression levels of one node on its target. The higher the value of α corresponding to a network edge, the stronger the epigenetic repression incorporated in that interaction. The underlying idea behind this framework is that epigenetic remodeling (or repression) serves as a self-stabilizing mechanism to maintain a cell-state and potentially propagate it across generations. In this epigenetic modeling framework, the longer a node stays at a high expression level ("ON") the less likely it is for the node to switch to a lower expression level ("OFF", due to chromatin and/or DNA methylation changes it may have mediated meanwhile), or in other words, the more likely a cell is to maintain the state driven by that master regulator, even if the levels of that node decline later. For instance, in fully matured Th1 cells, IFN-γ expression becomes relatively independent of T-bet activity and coincides with DNA methylation changes (Mullen *et al.*, 2002).

Here we use this framework to simulate multiple scenarios, i.e., epigenetic repression incorporated on various edges in a network, and quantify changes in phenotypic distribution in a differentiating T-cell population (Th1, Th2, Th17) in the presence of noise to account for stochastic effects. First, we considered the scenario of epigenetic repression mediated by one of the master regulators (say, B) on inhibitory links to other two nodes (from B to A and from B to C) (Figure 3A). The population distribution is calculated by considering multiple initial conditions (here 1000), each representing an individual cell. The trajectory of each initial condition (cell) is followed, and the expression values of A, B, and C are noted. Depending on the expression levels of the nodes, the state (of the cell) is defined and the population distribution is deduced. Noise is incorporated into the system at definite time intervals (see *Materials and Methods*). For a given tristable parameter set, we first identified population distribution in the absence of any epigenetic repression ($\alpha_{BA} = 0$, $\alpha_{BC} = 0$); ~20% cells were present in (high A, low B, low C) (Abc or state A) and 30% in (low A, high B, low C) (aBc or state B) states, while 50% cells exhibited a (low A, low B, high C) (abC or state C) phenotype (Figure 3B, left bottom panel).

As we increase the strength of epigenetic repression from B to C (α_{BC}), we observe a decrease in population percentage of abC (or C) state and a corresponding increase in that corresponding to A and B. At ($\alpha_{BA} = 0$, $\alpha_{BC} = 0.05$), the system displays a population percentage distribution of ~25% A, 45% B, and 30% C. This trend continues with a further increase in value of α_{BC}; at ($\alpha_{BA} = 0$, $\alpha_{BC} = 0.1$), a population distribution around 30% A, 45% B, and 25% C is observed (Figure 3B, left column). Incorporating epigenetic repression from B to A (α_{BA}) in addition to $\alpha_{BC} = 0.1$ further increases the population percentage corresponding to B. At ($\alpha_{BA} = 0.1$, $\alpha_{BC} = 0.1$), the population predominantly consists of cells in state B (70%) (Figure 3B, top row). This trend is further exemplified by the phase plot showing that the population percentage of B is minimum at low values of (α_{BA}, α_{BC}) and increases sharply as (α_{BA}, α_{BC}) values increase (Figure 3B). We performed a similar analysis for other tristable parameter sets and observed similar trends, although the degree of enrichment of corresponding state varied (Figure 3C; Supplemental Figures S2 and S3). For instance, in parameter sets P1, P3, and P4, including such epigenetic repression drastically alters the phenotypic distribution in favor of the master regulator which is inhibiting the other two epigenetically (C inhibits A and B in P1, B inhibits A and C in P3, B inhibits A and C in P4). The trends are consistent but not as strong, however, in parameter sets P2 (A inhibits B and C) and P5 (C inhibits A and B) (Supplemental Figures S2 and S3).

Put together, we conclude that including epigenetic repression from interactions originating from one of the three nodes in a toggle

triad helps to increase the percentage of cells in a state for which that node serves as a master regulator. The magnitude of change in phenotypic composition depends on the strength of epigenetic feedback of either or both interactions. Extrapolating these results in the context of T-cell differentiation, they imply that if T-bet can epigenetically repress on GATA3 and/or RORγT, the population predominantly will consist of Th1 cells. Similarly, Th2 (or Th17) cells can be the predominant phenotype in a heterogeneous T-cell population if GATA3 (or RORγT) can repress T-bet and RORγT (or T-bet and GATA3) epigenetically.

These observations offer dynamical insights into how the ability of RORγT to "not only establishing the permissive epigenetic landscape but also preventing the repressive one" (Lee *et al.*, 2020) is crucial for robust Th17 differentiation. Th17 cells have been reported to be relatively more plastic and can be reprogrammed readily to Th1 and Th2 (Lexberg *et al.*, 2008; Stadhouders *et al.*, 2018; Cerboni *et al.*, 2021) with implications in diseases such as rheumatoid arthritis (Yang *et al.*, 2019). This instability has been suggested to be driven by rapid epigenetic modifications for cytokines (*Il17a-Il17f, Ifng*) and TF (*Rorc*) gene expression associated with Th17 cell lineage specification (Mukasa *et al.*, 2010). Our simulations proposed that increased plasticity of Th17 cells may be a consequence of 1) weak epigenetic repression driven by RORγT on T-bet and/or GATA3, and/or 2) strong epigenetic repression mediated by T-bet and/or GATA3 on RORγT.

Impact of competing and complementing epigenetic repression driven by two master regulators on population distributions

Next, we consider the scenario of epigenetic repression incorporated on a pair of mutual repressive links (marked by green in Figure 4A: here inhibition between B and C is considered). The strength of epigenetic repression is characterized by corresponding α values α_{BC} and α_{CB}. For the given parameter set (P6), the system converges to ~ 20% A, 30% B, and 50% C in the absence of any epigenetic repression ($\alpha_{BC} = 0$, $\alpha_{CB} = 0$) (Figure 4A). Increasing either α_{BC} or α_{CB} increases the population percentage corresponding to state B or C, respectively; at ($\alpha_{BC} = 0.2$, $\alpha_{CB} = 0$), the population distribution is ~30% A, 45% B, and 25% C, while at ($\alpha_{BC} = 0$, $\alpha_{CB} = 0.3$), the heterogeneous population comprises 15% A, 15% B, and 70% C. Increasing both α_{BC} and α_{CB} values brings the population closer to the case of no epigenetic influence; at ($\alpha_{BC} = 0.2$, $\alpha_{CB} = 0.3$), the population distribution comprises ~25% A, 25% B, and 50% C. Quantifying the ratio of population percentages corresponding to states B and C with α_{BC} and α_{CB} as the two parameters, we observed skewed ratios of the two phenotypes when one of the epigenetic repression links is much stronger than the other (<1 at $\alpha_{BC} = 0.2$, $\alpha_{CB} = 0$; and >6 at $\alpha_{BC} = 0$, $\alpha_{CB} = 0.3$) (Figure 4B). Similar analysis for other parameter sets (Figure 4C; Supplemental Figures S4–S8) substantiates these trends where the ratio of population percentages of two representative states is skewed when one of the links dominates ([$\alpha_{1\text{-min}}$, $\alpha_{2\text{-max}}$] and [$\alpha_{1\text{-max}}$, $\alpha_{2\text{-min}}$]) but not when the epigenetic influence on one another is of comparable strengths ([$\alpha_{1\text{-min}}$, $\alpha_{2\text{-min}}$] and [$\alpha_{1\text{-max}}$, $\alpha_{2\text{-max}}$]). In the context of T-cell differentiation, these results imply that if T-bet and GATA3 can repress the expression or function of each other at an epigenetic level, the relative strength of their epigenetic inhibitions governs the relative proportions of Th1 and Th2 in a heterogeneous population. Similar statements can be made for mutual repression between any other pair of master regulators here.

Finally, we considered a scenario where both epigenetic repressions are incorporated on two edges terminating at a single node of the toggle triad (marked in green in Figure 4D; here inhibition of C by A and by B). The strength of the epigenetic feedback is characterized by corresponding α values, α_{AC} and α_{BC}, respectively. Without any epigenetic feedback ($\alpha_{AC} = 0$, $\alpha_{BC} = 0$), the system equilibrates to a population percentage distribution of 20% A, 30% B, and 50% C (Figure 4D). Increasing either α_{AC} or α_{BC} decreases the population percentage corresponding to state C (abC); at ($\alpha_{AC} = 0.1$, $\alpha_{BC} = 0$) and ($\alpha_{AC} = 0$, $\alpha_{BC} = 0.1$), the population percentage corresponding to state C drops to ~40 and 25%, respectively. Increasing both α_{AC} and α_{BC} further reduces the population percentage of state C (20% C at [$\alpha_{AC} = 0.1$, $\alpha_{BC} = 0.1$]) (Figure 4, D and E). Similar trends are seen for other parameter sets where one node is epigenetically being repressed by other two nodes: A inhibited by B and C epigenetically; C inhibited by A and B epigenetically; B inhibited by A and C epigenetically) (Figure 4F; Supplemental Figures S4–S8).

Together, these three different scenarios underscore how epigenetic repression incorporated through different inhibitory edges in T-bet/GATA3/RORγT regulatory network can alter the population distribution structure (the percentage of Th1, Th2, Th17) in a T-cell differentiation context.

The impact of epigenetic influence on population distribution depends on both corresponding strength(s) and duration(s)

So far, we have considered epigenetic feedback on any edge to not vary as a function of time. Next, we characterize the dynamics of the system with the epigenetic feedback provided only for a certain time duration instead of being present constantly (throughout the simulation) as previously.

We considered the tristable parameter set P6 where epigenetic repression was incorporated on two interactions originating from a single node (Figure 5A; B inhibiting both A and C; strengths: α_{BA} and α_{BC}, the same as the case considered in Figure 3). We switched on the epigenetic feedback for only a fraction of the entire simulation time (X). Without any epigenetic feedback, the population distribution converged to ~32% in states A and B and 36% in state C (Figure 5B). As X increased, the population percentage corresponding to state B increases while those corresponding to A and C simultaneously decrease. We then varied both parameters—X and α_{BA} (= α_{BC})—to make a phase plot. The population percentage corresponding to B is ~33% at $\alpha_{BA} = \alpha_{BC} = 0$ and no epigenetic feedback (X = 0). At low strengths ($\alpha_{BA} = \alpha_{BC} < 0.05$) and short durations (X < 0.5) of epigenetic feedback, the population distribution remains largely unperturbed (left bottom of Figure 5C). However, beyond this approximate threshold, increasing either the strength (dose) of epigenetic influence or the duration (marked by an asterisk and arrows in Figure 5C) leads to significant changes in the population levels corresponding to B.

Next, we considered the case where epigenetic influence was incorporated for mutual inhibition between two nodes (Figure 5D; B inhibiting C and C inhibiting B; strengths: α_{BC} and α_{CB}; same as the case considered in Figure 4, A and B). Without any epigenetic feedback, the population distribution converged to ~32% in both the states A and B and 36% in state C (Figure 5B). We started with the case where one of the two master regulators inhibited the other epigenetically (B inhibits C: $\alpha_{BC} = 0.2$, $\alpha_{CB} = 0$) and increased X (Figure 5E, left). The population percentage corresponding to C decreased (from ~37 to 20%) while that corresponding to B increased (from ~32 to 37%), although not drastically. We then considered the scenario of epigenetic repression through the other interaction (i.e., C inhibits B epigenetically, $\alpha_{BC} = 0$, $\alpha_{CB} = 0.3$), and estimated population distributions at varying values of X (Figure 5E, right). As

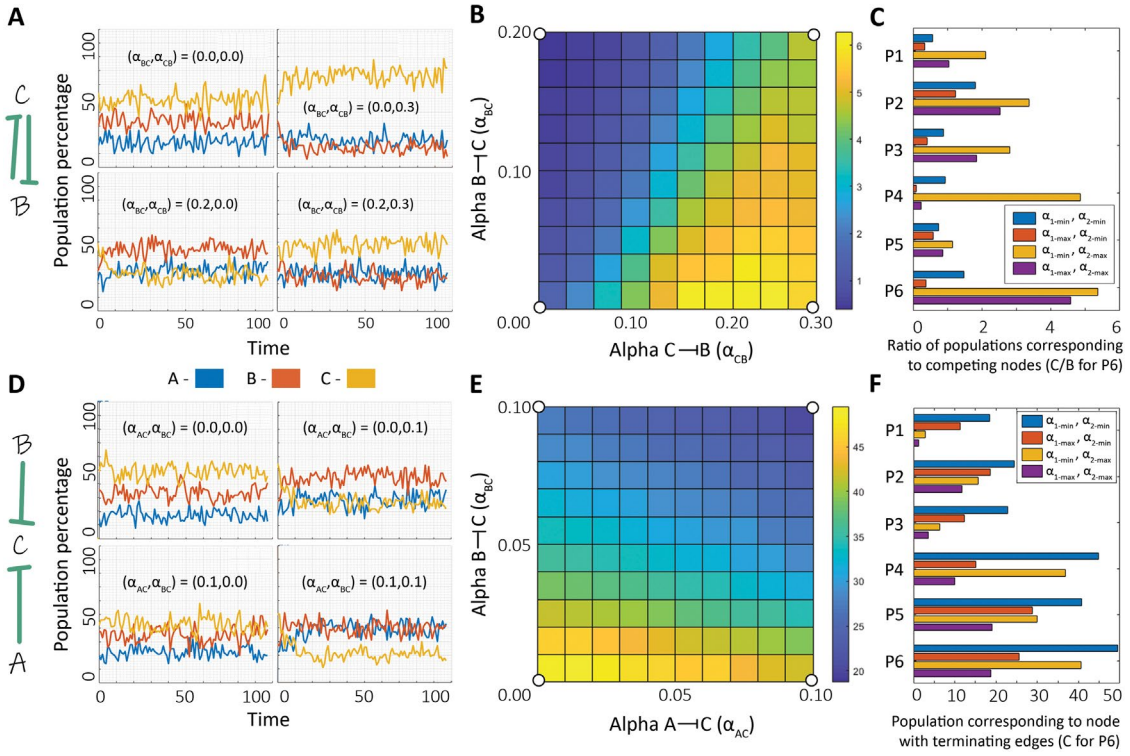

FIGURE 4: Epigenetic repression on edges originating from more than one node in the toggle triad. (A) (Left) Toggle triad network in which interactions where epigenetic repression is incorporated are marked in green. (Right) Dynamics of distribution of population percentage between states A, B, and C for certain pairs of α_{BC} and α_{CB} values. (B) Phase plot showing the ratio of population percentage of C to that of B with bifurcation parameters as the α values corresponding to the epigenetic feedback of B -| C and C -| B. (C) Ratio of population percentages of the nodes from which interactions with epigenetic feedback originate with pair of α values at combinations of maximum and minimum for three different parameter sets. (D) (Left) Same as A. (Right) Same as A but for certain values of α_{AC} and α_{BC}. (E) Phase plot showing the population percentage of C with bifurcation parameters as the α values corresponding to epigenetic feedback of A -| C and B -| C. (F) Population percentage of C (for parameter set P6), that of corresponding nodes in other parameter sets (P1–P5). Results for P6 are shown in B and E; those for P1-P5 are shown in Supplemental Figures S4–S8.

X increased, the population percentage corresponding to B dropped sharply (from ~32 to 20%) and that corresponding to C increased concurrently (from ~37 to 47%).

Next, to evaluate the impact of mutual epigenetic repression more clearly, we plotted a phase diagram by varying two parameters, X and the difference between epigenetic repressions that B and C have on each other (= $\alpha_{BC} - \alpha_{CB}$) (Figure 5F), showing the ratio of population percentages corresponding to states B and C. When both B and C inhibit each other comparably ($|\alpha_{BC} - \alpha_{CB}| < 0.05$), the population ratio remains largely unchanged irrespective of the duration of feedback X. On the other hand, when either interaction is much stronger than the other ($|\alpha_{BC} - \alpha_{CB}| >= 0.05$), the ratio of populations remains largely similar until the duration of epigenetic feedback crosses an approximate threshold (marked by asterisks), after which the population distribution diverges depending on the relative mutual strength of epigenetic influence.

Further, we considered the case with epigenetic repression incorporated on two interactions terminating on the same node (Figure 5G; A and B both inhibiting C; strengths: α_{AC} and α_{BC}; same as the case shown in Figure 5, D and E). Without any epigenetic influence, the population converged to ~32% cells in states A and B and 36% in state C (Figure 5H). As X is increased, the population percentage corresponding to state C decreases while that corresponding to states A and B concomitantly increase. When we varied both the parameters, X and α_{AC} (= α_{BC}), to draw a phase plot, we found that the population percentage corresponding to state C is ~38% at $\alpha_{BC} = \alpha_{AC} = 0$ and no epigenetic feedback (X = 0). At low strength ($\alpha_{BC} = \alpha_{AC} < 0.1$) and short durations (X < 0.5) corresponding to epigenetic repression, no major changes are observed for the population distribution (left bottom part in Figure 5I). However, beyond this approximate threshold (marked by an asterisk in Figure 5I), increasing either the strength or the duration (vertical and horizontal arrows in Figure 5I) leads to a comparable and pronounced decrease in the population corresponding to state C. Similar simulations for the three cases of epigenetic repression considered are performed for other parameter sets (P1–P5) and the trends remain consistent (Supplemental Figures S9–S13).

Put together, we conclude that both the factors—strength of epigenetic silencing (α) or the time duration for which it is switched on (X)—can act independently and alter the population distribution patterns, given a threshold amount of the other. These two variables seem to have additive and complementary effects rather than redundant ones. In terms of T-cell differentiation, these results indicate that either a strong epigenetic silencing of other cell lineages for a short duration or a gradually accumulating impact of epigenetic silencing (DNA methylation, histone modification etc.) can drive changes in the underlying population heterogeneity, suggesting an "area under the curve" dynamical principle.

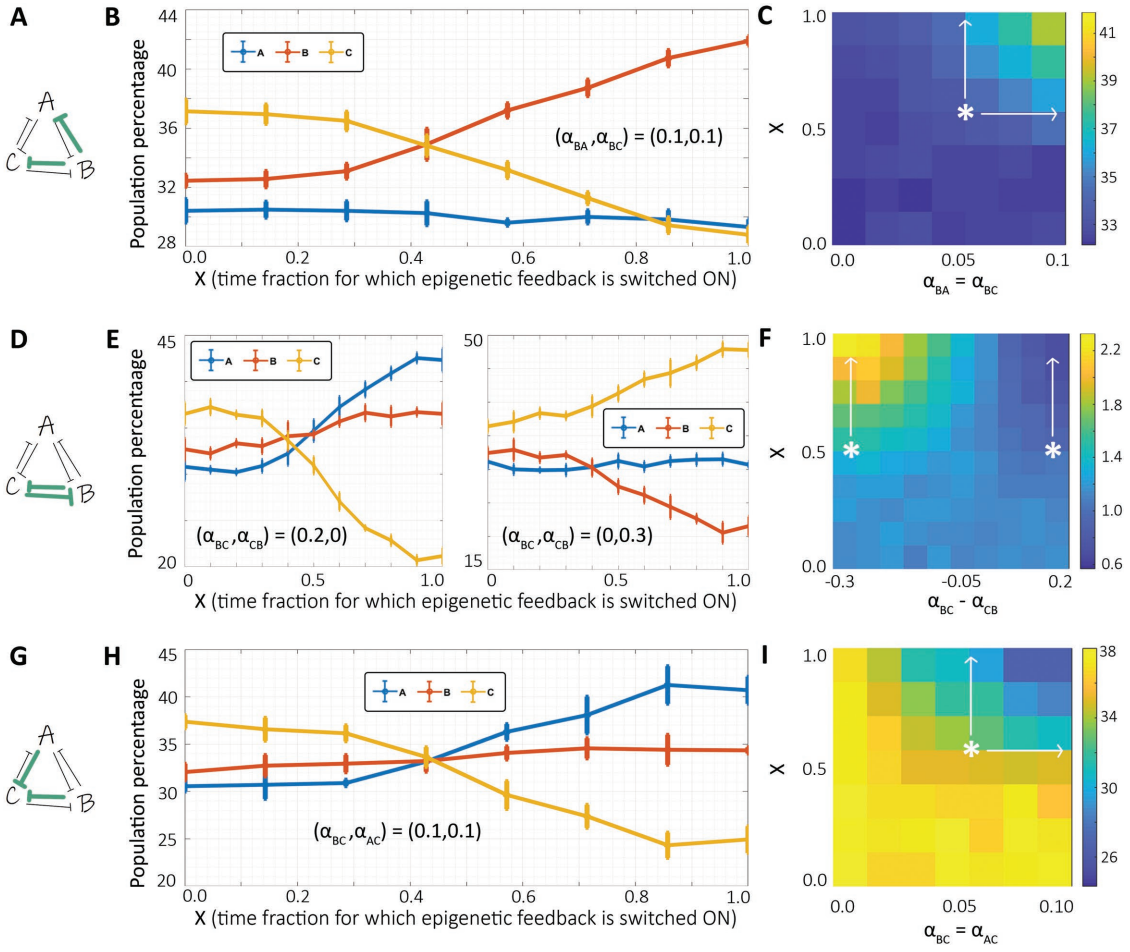

FIGURE 5: Epigenetic repression on edges originating from more than one node in the toggle triad. (A) Toggle Triad network topology in which interactions marked in green are being provided with epigenetic feedback. (B) Population percentages of A, B, and C as X, the fraction of time for which the epigenetic feedback for both marked interactions is switched ON and then turned OFF. (C) Phase plot showing population percentage of B (node from which interactions with epigenetic feedback originate) with bifurcation parameters as the α value corresponding to epigenetic feedback of B -| A and B -| C ($\alpha_{BA} = \alpha_{BC}$) and X. (D) Same as A. (E) Same as B but for two cases where feedback for one of the interactions, B -| C (C -| B) is switched ON with the other one C-|B (B-|C) switched OFF. (F) Phase plot showing ratio of population percentage of C to B (nodes between which interactions with epigenetic feedback are present) with bifurcation parameters as the difference of α values corresponding to the epigenetic feedback of B -| C and C -| B and X. (G) Same as A. (H) Same as B. (I) Phase plot showing population percentage of C (node onto which interactions with epigenetic feedback terminate) with bifurcation parameters as the α value corresponding to the epigenetic feedback of A-|C and B-|C (both same so considered on single axis) and X. Results for parameter set P6 shown here; those for P1–P5 are shown in Supplemental Figures S9–S13.

Previously, we considered varying values of $\alpha_{AC} = \alpha_{BC}$ and observed how this feedback strength and X affect the phenotypic heterogeneity of the population distribution. Next, we consider a more generic scenario where α_{AC} and α_{BC} values need not be identical. Also, instead of including the epigenetic influence on only incoming links on C (C being inhibited by A and B), we now also incorporate the epigenetic influence of C inhibiting A and/or B to represent the mutual epigenetic repression scenario.

First, we choose a tristable parameter set ({Abc, aBc, abC}) and include epigenetic influence from C to B with ($\alpha_{CB} = 0.2$). We can continuously decrease the strength of this influence, i.e., α_{CB} varies between 0 and 0.2, and increase the epigenetic influence from B on C (α_{BC}). Thus similarly to mutual repression as seen at a transcriptional level in a toggle switch (Gardner *et al.*, 2000), two nodes can also inhibit each other at an epigenetic level as well. The difference between the two parameters (α_{BC}–α_{CB}) indicates which epigenetic repression (from B to C or from C to B) is predominant. Thus we varied two parameters, α_{BC}–α_{CB} and X, and obtained the phase plots corresponding to percentage population in the three states: Abc (state A), aBc (state B), and abC (state C) (Figure 6A, i–iii, respectively). As α_{BC}–α_{CB} changes from –0.2 to 0.2, i.e., as the epigenetic influence of B inhibiting C takes over that of C inhibiting B, and given a minimal critical value of X (= 0.01), the population corresponding to state B increases from ~12 to ~20%. For the same change in parameters, population for state C decreases correspondingly from ~78 to ~70%. But, for the same change in epigenetic influence at a higher value of X (= 0.03), the change in population corresponding to state B is more drastic (from 12 to 40%), with a correspondingly sharp fall in population corresponding to state C (from 80 to 50%). Similar trends noted for a different representative example of mutual epigenetic repression are considered (i.e., when A and C inhibit each epigenetically) (Supplemental Figure S14A).

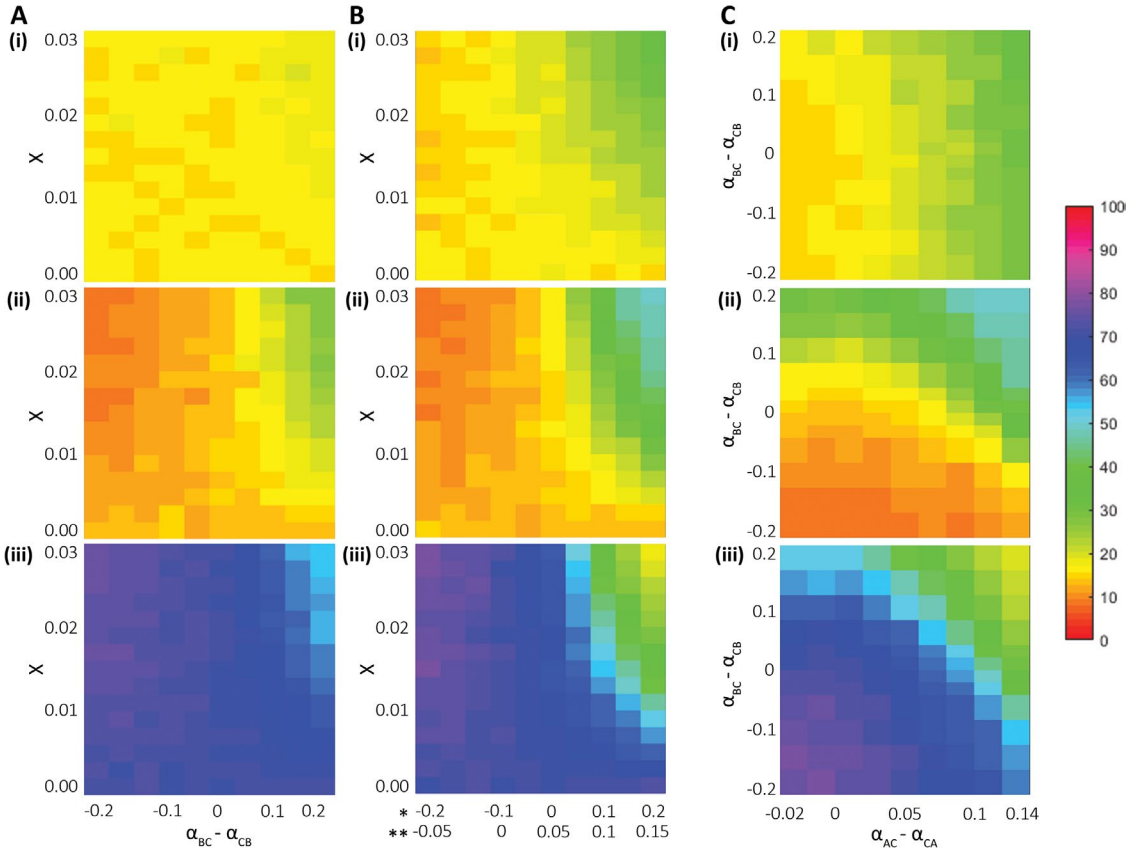

FIGURE 6: Varying the epigenetic repression onto the node in toggle triad. (A) (i) Phase plot of population percentage corresponding to node A with variations in two parameters: X and the relative epigenetic influence which is varied from a case of stronger repression from C to B ($\alpha_{BC} < \alpha_{CB}$) to a stronger repression from B to C ($\alpha_{BC} > \alpha_{CB}$) (ii) Same as i but for state B. (iii) Same as i but for state C. (B) (i) Same as Ai but for varying relative epigenetic influence in both feedback loops (between A and C and between B and C). Corresponding $\alpha_{BC} - \alpha_{CB}$ and $\alpha_{AC} - \alpha_{CA}$ values are given on the *x* axis marked by * and **, respectively. (ii) Same as i but for state B. (iii) Same as i but for state C. (C) (i) Phase plot of population percentage corresponding to state A with bifurcation parameters as the difference in α values corresponding to mutual epigenetic repression ($\alpha_{BC} - \alpha_{CB}$ and $\alpha_{AC} - \alpha_{CA}$), at $X = 0.03$. (ii) Same as i but for state B. (iii) Same as i but for state C. Results for parameter set P6 are shown here; those for P1–P5 parameter sets are shown in Supplemental Figures S14–S18.

Next, we investigate the scenario of mutual epigenetic repression for two toggle switches instead of just one: between B and C as well as between A and C. Thus in addition to changes in α_{BC}–α_{CB}, α_{AC}–α_{CA} can also be considered as a parameter to be varied. For this parameter set, while α_{BC}–α_{CB} changes from –0.2 to 0.2, α_{AC}–α_{CA} changes from –0.05 to 0.15. We observed that at X = 0.03, as the magnitude of the incoming epigenetic repression on C increases as compared with the ability of C to epigenetically repress A and/or B (i.e., α_{BC}–$\alpha_{CB} > 0$ and α_{AC}–$\alpha_{CA} > 0$), the population corresponding to state C drops sharply from 80 to 15% with a corresponding increase in population corresponding to both states A and B (from 10 to 35% for A and from 10 to 45% for B) (Figure 6B, i–iii).

Finally, we consider the case of a fixed duration for which epigenetic repression is switched ON (X = 0.03), but we vary the difference in the strengths of epigenetic repression between two master regulators to draw the phase plot of population corresponding to the three states (Figure 6C). We noticed that for this parameter set, the population corresponding to state A changes more along the *x* axis (α_{AC}–α_{CA}) than along the *y* axis (α_{BC}–α_{CB}), i.e., the frequency of state A is more sensitive to changes in mutual epigenetic repression between A and C than those between B and C (Figure 6Ci). A similar trend is seen for node B initially (i.e., a change in the frequency of state B is more prominent along the *y* axis [α_{BC}–α_{CB}] than along the *x* axis [α_{AC}–α_{CA}]), but at higher values of α_{AC}–α_{CA}, the population corresponding to state B is also affected (Figure 6C, ii). Because C is involved in both instances of mutual epigenetic repression (i.e., with B and with A), the population corresponding to state C falls with an increase in incoming epigenetic repression from either node—A or B. When C is maximally repressing A and B at an epigenetic level (left bottom part of Figure 6Ciii), the population corresponding to state C is 80%. At the values corresponding to (maximum α_{AC}, minimum α_{BC}) and (minimum α_{AC}, maximum α_{BC}) (right bottom and left top parts of Figure 6Ciii respectively), the population corresponding to state C falls to 60 and 55%, respectively. At the value corresponding to (maximum α_{AC}, maximum α_{BC}), the population of C decreases to 15% (top right part of Figure 6Ciii). Besides depending on the difference in corresponding α values, changes in population distribution can depend on X too (Supplemental Figure S6, B and C). These simulations performed for other parameter sets (P1–P5) reveal consistent trends (Supplemental Figures S14–S18).

In terms of T-cell differentiation, these results imply that if the extent of epigenetic repression on one of the three master regulators is strong enough as compared with the repression it can mediate on one or both of other two master regulators, the corresponding phenotypic frequency will decrease majorly.

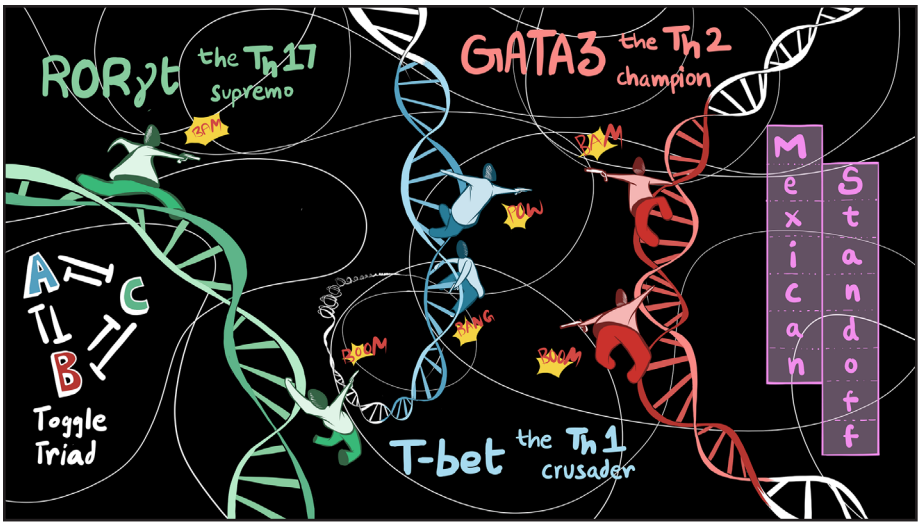

FIGURE 7: A schematic representing Th1/Th2/Th17 differentiation mediated by a toggle triad.

DISCUSSION

Gaining a predictive understanding of the dynamics of cell-fate decisions is instrumental for decoding cell differentiation during development and homeostasis and modulating it in pathological scenarios. Cell-fate decisions, including those seen in naïve helper T-cell differentiation into Th1, Th2, and Th17 cells, are the emergent outcomes of an entangled interplay of various levels of regulatory control—transcriptional (Evans and Jenner, 2013; Pillai and Jolly, 2021), translational (Liu *et al.*, 2018; Sarkar *et al.*, 2019), alternative splicing (Jolly *et al.*, 2018; Radens *et al.*, 2021), epigenetic (Wilson *et al.*, 2009; Jia *et al.*, 2019), and metabolic (Stark *et al.*, 2019; Jia *et al.*, 2021) among others. Recent efforts have begun to identify the dynamics of cell-fate decisions by investigating time-course transcriptional data (Pedicini *et al.*, 2010; Intosalmi *et al.*, 2015; Cook and Vanderhyden, 2020; Deshmukh *et al.*, 2021). However, how the different regulatory layers operating at varying time scales orchestrate coordinated cell decision-making at an individual cell and cell population level remains largely unclear.

Here we investigate the dynamics of coupled transcriptional-epigenetic regulation in a network of three mutually repressing nodes forming a toggle triad (Figure 7). Analyzing the dynamics of a toggle triad can help elucidate CD4+ helper T-cell differentiation into Th1, Th2, and Th17 cells given that each of the master regulator (T-bet, GATA3, and RORγT) can repress the other two at transcriptional and/or epigenetic levels directly or indirectly. We incorporated a simple phenomenological model to include epigenetic influence (Miyamoto *et al.*, 2015) to demonstrate how varying strengths of epigenetic repression can alter the stability of the three cell states (Th1, Th2, and Th17) and consequently alter the proportion of these phenotypes in a differentiating CD4+ T-cell population. The stronger the epigenetic repression mediated by a master regulator the higher the predominance of corresponding phenotype in a cell population.

Our model predicts that besides its strength, the duration for which epigenetic repression is "active" can modulate the population heterogeneity during helper T-cell differentiation. Specifically, a weaker epigenetic repression for longer times and a stronger repression for shorter times has similar outcomes; this prediction can help plan next experiments to decode T-cell differentiation as a function of varying cytokine doses and durations. Thus unlike previous mathematical models for CD4+ T-cell differentiation mostly focused on steady-state analysis at a transcriptional level (Hong *et al.*, 2011; Martinez-Sanchez *et al.*, 2018; Puniya *et al.*, 2018), our model incorporates the epigenetic-driven dynamics of plasticity and heterogeneity among Th1, Th2, and Th17 phenotypes in a CD4+ T-cell population.

Phenotypic heterogeneity has been reported in silico (Martinez-Sanchez *et al.*, 2018; Puniya *et al.*, 2018), in vitro, and in vivo in the presence of a mixture of cytokines driving different T-cell phenotypes (Han *et al.*, 2014; Becattini *et al.*, 2015; DuPage and Bluestone, 2016; Eizenberg-Magar *et al.*, 2017; DiToro and Basu, 2021; van Beek *et al.*, 2021). Our model predicts that multistability in T-bet/GATA3/ RORγT regulatory network can allow for phenotypic switching and heterogeneity as its inherent dynamical property, similar to other regulatory networks driving sibling cell fates (Zhou and Huang, 2011). Another dynamical feature of multistable systems is the presence of both stability (for individual phenotypes) and plasticity (among many phenotypes), and epigenetic remodeling may alter the balance between them. For instance, differences in chromatin marks may alter the propensity of an epithelial cell to switch to a mesenchymal phenotype under the influence of an inducer (Eichelberger *et al.*, 2020; Jia *et al.*, 2020). Similarly, a subset of Th2 cells have been shown to not express T-bet and IFNγ when stimulated under Th1 conditions (Messi *et al.*, 2003). Recent "cross-polarization" experiments highlighted such "limited but detectable functional plasticity" for a population of Th1, Th2, and Th17 cells, indicating that these phenotypes represent relatively stable entities (Tortola *et al.*, 2020). Epigenetic marks are considered to help maintain such stability and heritability of cell-fate decisions (Wilson *et al.*, 2009), but whether epigenetic differences underlie such heterogeneity in response (stability vs. plasticity) in a cell population needs further investigation (van Beek *et al.*, 2021). Preliminary evidence in Th1 cells pinpoints that permissive chromatin modifications coincide with the ability of Th1 cells to express IL-17 under Th17-polarizing conditions (Curtis *et al.*, 2010), but it falls short of establishing a causative connection. Our model simulations imply that epigenetic repression driven by master regulators can influence the rate of switching from one phenotype to another, thus offering a quantitative dynamic platform to measure the stability (heritability) versus plasticity propensities.

The balance between plasticity and stability is likely to depend on phenotype-specific global mapping of chromatin marks such as H3K4me3 and H3K27me3 that associate with activation and repression of gene expression, respectively (Wei *et al.*, 2009). Higher plasticity has been shown to be concurrent with the presence of bivalent chromatin (i.e., simultaneous presence of active and repressive marks) (Chaffer *et al.*, 2013). For instance, the *Foxp3* promoter is not epigenetically repressed in Th17 cells, possibly enabling Th17-Treg plasticity (Wei *et al.*, 2009). In our phenomenological model which does not explicitly capture the molecular details of epigenetic repression (Huang and Lei, 2019; Zhao *et al.*, 2021), a bivalent chromatin state can be conceptually mapped onto the regions of relatively weak epigenetic influence of one master regulator on others. Thus the weaker the epigenetic influence of node A on node B (α_{AB}) relative to that of node B on node A (α_{BA}) the higher the expected plasticity of the phenotype driven by node A. Indeed, this trend is

observed in our simulations in terms of both plasticity of phenotype and the consequent population distribution. Therefore our model can possibly explain the high plasticity observed for Th17 cells observed in many contexts such as cancer and autoimmunity (Stadhouders *et al.*, 2018; Cerboni *et al.*, 2021). In other words, we propose that increased plasticity of Th17 cells may be a consequence of 1) weak epigenetic repression driven by RORγT on T-bet and/or GATA3 and/or 2) strong epigenetic repression mediated by T-bet and/or GATA3 on RORγT.

Together, despite the limitations of investigating a minimalistic regulatory network and incorporating epigenetic influence only at a phenomenological level, our model simulations offer valuable insights into the dynamics of phenotypic plasticity and heterogeneity in a CD4+ T-cell population comprising Th1, Th2, and Th17 phenotypes. We provide a platform to quantify the plasticity and stability of different phenotypes and the overall phenotypic distribution as a function of varying strengths of epigenetic influence mediated by the master regulators (T-bet, GATA3, RORγT) on one another in a toggle triad (Figure 6). Various instances of plasticity among Th1, Th2, and Th17 phenotypes have been seen depending on the microenvironment (Krawczyk *et al.*, 2007; Zhou *et al.*, 2009; Geginat *et al.*, 2016; Kanamori *et al.*, 2018; Tortola *et al.*, 2020), but whether this switching happens back and forth (for instance, Th1 being converted to Th2 and converting back to Th1 on the removal of signal) remains to be investigated. The extent of such reversibility can depend on, among other factors, duration and dose of inducing signals as well as a chromatin state of various regulators (Stadhouders *et al.*, 2018), as seen in other cell-fate decision-making scenarios (Jia *et al.*, 2019; Katsuno *et al.*, 2019; Eichelberger *et al.*, 2020). Our model simulations provide a framework to understand the possible conditions that may be needed for bidirectional transitions in the form of intrinsic (epigenetic regulation) and/or extrinsic (cytokine) factors.

Our next steps include extending this T-bet/GATA3/RORγT toggle triad network to include the master regulators of other lineages that CD4+ T-cells can differentiate into, such as induced T-regulatory cells (iTregs) and T follicular helper (Tfh) cells among others (Martinez-Sanchez *et al.*, 2018). It would be intriguing to observe what network topologies are required to explain this diversity of phenotypic repertoire of T-cells. The design principles learned through such analysis can not only reveal the dynamics of CD4+ T-cell differentiation but also guide the design of multistable synthetic gene regulatory circuits (Santos-Moreno *et al.*, 2020; Zhu *et al.*, 2022).

MATERIALS AND METHODS

Request a protocol through *Bio-protocol*.

RACIPE (RAndom CIrcuit PErturbation analysis)

RACIPE is a computational tool that investigates the emergent dynamics of a given network topology (Huang *et al.*, 2017) which takes network topology as an input. Rather than specifying certain kinetic parameters of the system, RACIPE attempts to reveal all possible behaviors of the system by sampling these parameters over a range and simulating the model multiple times with varying parameter sets and initial conditions. The analysis of these results provides information on the relation between the behavior or states of the topology enabled by specific parametric spaces as well as the frequency or probability of different behaviors and states/phases of the network.

The formulation of interactions between two nodes in the network, say a node A being inhibited by a node B, in RACIPE is given by the following equation:

$$\frac{dA}{dt} = g_A * H^s\left(B, B^0A, nBA, \lambda BA\right) - k_A * A$$

where g_A and k_A are intrinsic production and degradation rates of node A, respectively, and the Hill function H^s (B, B^0 A, *nBA, λBA*) represents the interaction (here inhibition) of node B on node A. Thus the first term on RHS of the equation dictates the net production rate of the node A, while the second term of the equation dictates the degradation rate.

The interaction term is further expanded as

$$H^s\left(B, B^0A, nBA, \lambda BA\right) = H^-(B) + \lambda BA^*\left(1 - H^-(B)\right)$$

$$\text{where, } H^-(B) = \frac{1}{1+\left(\frac{B}{B^0A}\right)^{nBA}}$$

The base formulation uses Hill function but is modified to include both activation/inhibition into the same equation rather than using two separate ones. The usage of Hill functions to represent the inhibition or activation between genes is a consequence of using a biochemical rate equation formulation of gene expression (Edelstein-Keshet, 2005; Santillan, 2008). In this formulation, called a shifted Hill function (Lu *et al.*, 2013), the parameters include the threshold (B^0 *A*), Hill coefficient (*nBA*), and fold-change value (*λBA*). The threshold determines the expression level of node B over which the inhibitory link from node B to node A is more active. Decreasing the threshold activates the link even at low expression levels of node B. The Hill coefficient determines how quickly the effect of inhibition escalates with an increasing expression level of node B (cooperativity) while the fold-change value determines the degree of the effect of inhibition (or activation).

Apart from the network topology as an input, the number of parameter sets and the number of initial conditions per parameter set can be input; their default values are 10,000 and 100, respectively). Default values (given below) of sampling ranges for parameters can also be modified for different simulations. Default values of g and k are between (1,100) and (0.1, 1), respectively; the Hill coefficient is sampled from the set {1,2,3,4,5,6}; the fold-change value is sampled from (1,100) for activation and (0.01, 1) for inhibition. The threshold is calculated such that for all the parameter sets of the RACIPE model ensemble, each interaction has a roughly 50% chance of being functional (Huang *et al.*, 2017). A parameter set is classified as enabling monostability, bistability, tristability, etc. depending on the number of different steady states the 1000 initial conditions that the system converges to at the end of simulation.

For the purpose of this paper, we have only shortlisted parameter sets which enabled tristability with the states as {Abc, aBc, abC}. Additionally, we placed a criterion of at least 20% of the initial conditions ending up in all three of the states to focus on parameter sets with comparable relative stability of the three states. We then selected few representative parameter sets for performing simulations shown in this paper.

Mathematical framework for epigenetic feedback

The formalism used for epigenetic feedback tries to emulate the process at a phenomenological level. The referred phenomenon is that the longer a node stays at high expression, the higher the chance it has to stay high (Miyamoto *et al.*, 2015) potentially because with epigenetic remodeling it is capable of ensuring which may repress its inhibitors via chromatin changes, as seen for various cell-fate decision cases (Díaz-López *et al.*, 2015;

Somarelli *et al*., 2016). We introduced an epigenetic parameter (α) to quantify the threshold (half-maximal) levels corresponding to influence of expression levels of one node on the other two. The higher the value of α the lower the threshold of corresponding shifted Hill function (Miyamoto *et al*., 2015). This epigenetic feedback is added to the threshold instead of Hill coefficient or fold-change value because it tells us about the levels of the node which epigenetically influences its target.

The equations used are as follows:

$$A(i+1) = A(i) + \tau * \left[g_A * H\left(B, B^0A, nBA, \lambda BA\right) * H\left(C, C^0A, nCA, \lambda CA\right) - k_A \cdot A \right] + normrnd\left(0, 1, [1,3]\right)^* N$$

$$A^0B(i+1) = A^0B(i) + \tau * [a^0b - A^0B(i) - \left(\alpha_{AB} * A(i)\right)] * \frac{1}{\beta}$$

The first equation is the form of the iterative equation used for the expression level of a node. $A(i + 1)$ and $A(i)$ represent the node A expression levels at consecutive iterations; τ represents the size of the time-step taken. In the equation, g_A and k_A are the intrinsic production and degradation rates of node A, respectively. H^s (B, B^0 A, nBA, λBA) and H (C, C^0 A, nCA, λCA) represent the interaction (here inhibition) of nodes B and C on node A, respectively. The last term is the noise added to the system at set intervals in the iteration. Every time noise is added, random numbers in a vector of size 1×3 are generated from a normal distribution with mean and variance 0 and 1, respectively (noise is added to all three nodes). These random numbers are multiplied by N (which is an order of magnitude lower to the mean expression level of nodes) to correspond to expression levels of the nodes. Formulation of a white noise term can capture different sources of biological noise such as noise due to transcriptional bursting, chromatin accessibility, and protein or mRNA degradation. This formalism has previously been used to approximate biological noise (Tkacik *et al*., 2009).

The second equation represents how epigenetic feedback is employed in the formalism. Here feedback is provided to the inhibition of node A on node B. $A^0B(i + 1)$ and $A^0B(i)$ represent threshold values corresponding to the inhibition of node B by node A at consecutive iterations; a^0b is the set threshold value given by the chosen parameter set (i.e., without any epigenetic feedback); α_{AB} is epigenetic parameter providing feedback corresponding to the node expression level $A(i)$. The higher the α value the stronger the epigenetic feedback provided or the lower the steady-state threshold value is. The longer the node A is expressed high the lower the threshold level A^0B goes. Thus even if the levels of node A drop due to various factors, because the threshold value is very low (representing the condition in which chromatin remodeling has taken place), the inhibition of node A on node B is still active, thus enabling node A to recover its high expression while making sure that the expression of node B remains low. β is a scaling factor for determining the rate of change of the threshold value and is used to control abrupt changes in node expression.

sRACIPE

We used the webserver facility of Gene Circuit Explorer (GeneEx) to simulate stochastic dynamics of gene regulatory circuits: https://geneex.jax.org/. The tool tries to account for stochastic effects due to cell-to-cell variation and low copy numbers in individual cells by including a noise term based on a Wiener process (Wt) with a variance. The stochastic differential equation are solved using the Euler-Maruyama method (Kohar and Lu, 2018).

Scoring of Th1, Th2, and Th17 gene signatures

To calculate the activity scores for specific signatures, the ssGSEA metric (Barbie *et al*., 2009) was used on gene lists of the Th1, Th2, and Th17 cell types obtained (Supplemental Table S3 in Radens *et al*., 2020). We also computed average z-scores to be used as a metric of quantification for dataset GSE62484.

ACKNOWLEDGMENTS

We thank Mr. Navin Vincent (IISc Bangalore) for help with the phase diagrams in Figure S1. M.K.J. was supported by Ramanujan Fellowship (SB/S2/RJN-049/2018) awarded by the Science and Engineering Research Board (SERB), Department of Science and Technology (DST), Government of India, and by InfoSys Young Investigator Fellowship awarded by Infosys Foundation, Bangalore. A.S.D. acknowledges support by Prime Ministers' Research Fellowship (PMRF) awarded by the Government of India.

REFERENCES

Äijö T, Edelman SM, Lönnberg T, Larjo A, Kallionpää H, Tuomela S, Engström E, Lahesmaa R, Lähdesmäki H (2012). An integrative computational systems biology approach identifies differentially regulated dynamic transcriptome signatures which drive the initiation of human T helper cell differentiation. BMC Genomics 13, 572.

Barbie DA, Tamayo P, Boehm JS, Kim SY, Moody SE, Dunn IF, Schinzel AC, Sandy P, Meylan E, Scholl C, *et al*. (2009). Systematic RNA interference reveals that oncogenic KRAS-driven cancers require TBK1. Nature 462, 108–112.

Bargaje R, Trachana K, Shelton MN, McGinnis CS, Zhou JX, Chadick C, Cook S, Cavanaugh C, Huang S, Hood L (2017). Cell population structure prior to bifurcation predicts efficiency of directed differentiation in human induced pluripotent cells. Proc Natl Acad Sci USA 114, 2271–2276.

Baumann V, Wiesbeck M, Breunig CT, Braun JM, Köferle A, Ninkovic J, Götz M, Stricker SH (2019). Targeted removal of epigenetic barriers during transcriptional reprogramming. Nat Commun 10, 2119.

Becattini S, Latorre D, Mele F, Foglierini M, De Gregorio C, Cassotta A, Fernandez B, Kelderman S, Schumacher TN, Corti D, *et al*. (2015). T cell immunity. Functional heterogeneity of human memory CD4$^+$ T cell clones primed by pathogens or vaccines. Science 347, 400–406.

van Beek JJP, Rescigno M, Lugli E (2021). A fresh look at the T helper subset dogma. Nat Immunol 22, 104–105.

Cerboni S, Gerhmann U, Preite S, Mitra S (2021). Cytokine-regulated Th17 plasticity in human health and diseases. Immunology 163, 3–18.

Chaffer CL, Marjanovic ND, Lee T, Bell G, Kleer CG, Reinhardt F, D'Alessio AC, Young RA, Weinberg RA (2013). Poised chromatin at the ZEB1 promoter enables breast cancer cell plasticity and enhances tumorigenicity. Cell 154, 61–74.

Chang S, Aune M (2007). Dynamic changes in histone-methylation "marks" across the locus encoding interferon-gamma during the differentiation of T helper type 2 cells. Nat Immunol 8, 723–731.

Chatterjee S, Daenthanasanmak A, Chakraborty P, Wyatt MW, Dhar P, Selvam SP, Fu J, Zhang J, Nguyen H, Kang I, *et al*. (2018). CD38-NAD + axis regulates immunotherapeutic anti-tumor T cell response. Cell Metab 27, 85–100.e8.

Cherry JL, Adler FR (2000). How to make a biological switch. J Theor Biol 203, 117–133.

Cook DP, Vanderhyden BC (2020). Context specificity of the EMT transcriptional response. Nat Commun 11, 2142.

Curtis MM, Rowell E, Shafiani S, Negash A, Urdahl KB, Wilson CB, Way SS (2010). Fidelity of pathogen-specific CD4+ T cells to the Th1 lineage is controlled by exogenous cytokines, interferon-γ expression, and pathogen lifestyle. Cell Host Microbe 8, 163–173.

Deshmukh AP, Vasaikar SV, Tomczak K, Tripathi S, den Hollander P, Arslan E, Chakraborty P, Soundararajan R, Jolly MK, Rai K, *et al*. (2021). Identification of EMT signaling cross-talk and gene regulatory networks by single-cell RNA sequencing. Proc Natl Acad Sci USA 118, e2102050118.

Díaz-López A, Díaz-Martín J, Moreno-Bueno G, Cuevas EP, Santos V, Olmeda D, Portillo F, Palacios J, Cano A (2015). Zeb1 and Snail1 engage miR-200f transcriptional and epigenetic regulation during EMT. Int J Cancer 136, E62–E73.

DiToro D, Basu R (2021). Emerging Complexity in CD4+T lineage programming and its implications in colorectal cancer. Front Immunol 12, 694833.

Duddu AS, Sahoo S, Hati S, Jhunjhunwala S, Jolly MK (2020). Multi-stability in cellular differentiation enabled by a network of three mutually repressing master regulators. J R Soc Interface 17, 20200631.
DuPage M, Bluestone JA (2016). Harnessing the plasticity of CD4+ T cells to treat immune-mediated disease. Nat Rev Immunol 16, 149–163.
Edelstein-Keshet L (2005). Mathematical Models in Biology, Philadelphia: SIAM.
Eichelberger L, Saini M, Moreno HD, Klein C, Bartsch JM, Falcone M, Reitberger M, Espinet E, Vogel V, Graf E, *et al.* (2020). Maintenance of epithelial traits and resistance to mesenchymal reprogramming promote proliferation in metastatic breast cancer. BioRxiv, 998823.
Eizenberg-Magar I, Rimer J, Zaretsky I, Lara-Astiaso D, Reich-Zeliger S, Friedman N (2017). Diverse continuum of CD4+ T-cell states is determined by hierarchical additive integration of cytokine signals. Proc Natl Acad Sci USA 114, E6647–E6456.
Evans CM, Jenner RG (2013). Transcription factor interplay in T helper cell differentiation. Brief Funct Genomics 12, 499–511.
Fang D, Zhu J (2017). Dynamic balance between master transcription factors determines the fates and functions of CD4 T cell and innate lymphoid cell subsets. J Exp Med 214, 1861–1876.
Gardner TS, Cantor CR, Collins JJ (2000). Construction of a genetic toggle switch in Escherichia coli. Nature 403, 339–342.
Geginat J, Paroni M, Kastirr I, Larghi P, Pagani M, Abrignani S (2016). Reverse plasticity: TGF-β and IL-6 induce Th1-to-Th17-cell transdifferentiation in the gut. Eur J Immunol 46, 2306–2310.
Graham TGW, Tabei SMA, Dinner AR, Rebay I (2010). Modeling bistable cell-fate choices in the Drosophila eye: Qualitative and quantitative perspectives. Development 137, 2265–2278.
Gustafsson M, Gawel DR, Alfredsson L, Baranzini S, Björkander J, Blomgran R, Hellberg S, Eklund D, Ernerudh J, Kockum I, *et al.* (2015). A validated gene regulatory network and GWAS identifies early regulators of T cell-associated diseases. Sci Transl Med 7, 313ra178.
Han A, Glanville J, Hansmann L, Davis MM (2014). Linking T-cell receptor sequence to functional phenotype at the single-cell level. Nat Biotechnol 32, 684–692.
Hari K, Sabuwala B, Subramani BV, La Porta CAM, Zapperi S, Font-Clos F, Jolly MK (2020). Identifying inhibitors of epithelial-mesenchymal plasticity using a network topology based approach. Npj Syst Biol Appl 6, 15.
Hertweck A, Evans CM, Eskandarpour M, Lau JC, Oleinika K, Jackson I, Kelly A, Ambrose J, Adamson P, Cousins DJ, *et al.* (2016). T-bet Activates Th1 Genes through Mediator and the Super Elongation Complex. Cell Rep 15, 2756–2770.
Hirahara K, Vahedi G, Ghoreschi K, Yang XP, Nakayamada S, Kanno Y, O'Shea JJ, Laurence A (2011). Helper T-cell differentiation and plasticity: Insights from epigenetics. Immunology 134, 235–245.
Hong T, Xing J, Li L, Tyson JJ (2011). A Mathematical model for the reciprocal differentiation of T helper 17 cells and induced regulatory T cells. PLoS Comput Biol 7, e1002122.
Huang B, Lu M, Jia D, Ben-Jacob E, Levine H, Onuchic JN (2017). Interrogating the topological robustness of gene regulatory circuits by randomization. PLoS Comput Biol 13, e1005456.
Huang R, Lei J (2019). Cell-type switches induced by stochastic histone modification inheritance. Discret Contin Dyn Syst Ser B 24, 5601–5619.
Huang S, Guo YP, May G, Enver T (2007). Bifurcation dynamics in lineage-commitment in bipotent progenitor cells. Dev Biol 305, 695–713.
Intosalmi J, Ahlfors H, Rautio S, Mannerstöm H, Chen ZJ, Lahesmaa R, Stockinger B, Lähdesmäki H (2015). Analyzing Th17 cell differentiation dynamics using a novel integrative modeling framework for time-course RNA sequencing data. BMC Syst Biol 9, 81.
Jia D, Park JH, Kaur H, Jung KH, Yang S, Tripathi S, Galbraith M, Deng Y, Jolly MK, Kaipparettu BA, *et al.* (2021). Towards decoding the coupled decision-making of metabolism and epithelial-to-mesenchymal transition in cancer. Br J Cancer 124, 1902–1911.
Jia W, Deshmukh A, Mani SA, Jolly MK, Levine H (2019). A possible role for epigenetic feedback regulation in the dynamics of the epithelial-mesenchymal transition (EMT). Phys Biol 16, 066004.
Jia W, Tripathi S, Chakraborty P, Chedere A, Rangarajan A, Levine H, Jolly MK (2020). Epigenetic feedback and stochastic partitioning during cell division can drive resistance to EMT. Oncotarget 11, 2611–2624.
Jolly MK, Preca B-T, Tripathi SC, Jia D, George JT, Hanash SM, Brabletz T, Stemmler MP, Maurer J, Levine H (2018). Interconnected feedback loops among ESRP1, HAS2, and CD44 regulate epithelial-mesenchymal plasticity in cancer. APL Bioeng 2, 031908.
Josefowicz SZ (2013). Regulators of chromatin state and transcription in CD4 T-cell polarization. Immunology 139, 299–308.
Kaiko GE, Horvat JC, Beagley KW, Hansbro PM (2008). Immunological decision-making: How does the immune system decide to mount a helper T-cell response? Immunology 123, 326–338.
Kanamori M, Nakatsukasa H, Ito M, Chikuma S, Yoshimura A (2018). Reprogramming of Th1 cells into regulatory T cells through rewiring of the metabolic status. Int Immunol 30, 357–373.
Kanduri K, Tripathi S, Larjo A, Mannerström H, Ullah U, Lund R, Hawkins RD, Ren B, Lähdesmäki H, Lahesmaa R (2015). Identification of global regulators of T-helper cell lineage specification. Genome Med 7, 122.
Katsuno Y, Meyer DS, Zhang Z, Shokat KM, Akhurst RJ, Miyazono K, Dernyck R (2019). Chronic TGF-β exposure drives stabilized EMT, tumor stemness, and cancer drug resistance with vulnerability to bitopic mTOR inhibition. Sci Signal 12, eaau8544.
Kohar V, Lu M (2018). Role of noise and parametric variation in the dynamics of gene regulatory circuits. Npj Syst Biol Appl 4, 40.
Krawczyk CM, Shen H, Pearce EJ (2007). Functional plasticity in memory T helper cell responses. J Immunol 178, 4080–4088.
Lee S, Kim J, Min H, Seong RH (2020). RORγt-driven TH17 cell differentiation requires epigenetic control by the Swi/Snf chromatin remodeling complex. IScience 23, 101106.
Lexberg MH, Taubner A, Förster A, Albrecht I, Richter A, Kamradt T, Radbruch A, Chang HD (2008). Th memory for interleukin-17 expression is stable in vivo. Eur J Immunol 38, 2654–2664.
Liu C, Yang H, Shi W, Wang T, Ruan Q (2018). MicroRNA-mediated regulation of T helper type 17/regulatory T-cell balance in autoimmune disease. Immunology 155, 427–434.
Lu M, Jolly MK, Gomoto R, Huang B, Onuchic J, Ben-Jacob E (2013). Tristability in cancer-associated microRNA-TF chimera toggle switch. J Phys Chem B 117, 13164–13174.
Martinez-Sanchez ME, Huerta L, Alvarez-Buylla ER, Luján CV (2018). Role of cytokine combinations on CD4+ T cell differentiation, partial polarization, and plasticity: Continuous network modeling approach. Front Physiol 9, 877.
Messi M, Giacchetto I, Nagata K, Lanzavecchia A, Natoli G, Sallusto F (2003). Memory and flexibility of cytokine gene expression as separable properties of human TH1 and TH2 lymphocytes. Nat Immunol 4, 78–86.
Miyamoto T, Furusawa C, Kaneko K (2015). Pluripotency, differentiation, and reprogramming: a gene expression dynamics model with epigenetic feedback regulation. PLoS Comput Biol 11, e1004476.
Mukasa R, Balasubramani A, Lee YK, Whitley SK, Weaver BT, Shibata Y, Crawford GE, Hatton RD, Weaver CT (2010). Epigenetic instability of cytokine and transcription factor gene loci underlies plasticity of the T helper 17 cell lineage. Immunity 32, 616–627.
Mullen AC, Hutchins AS, High FA, Lee HW, Sykes KJ, Chodosh LA, Reiner SL (2002). Hlx is induced by and genetically interacts with T-bet to promote heritable THI gene induction. Nat Immunol 3, 652–658.
Nashun B, Hill PW, Hajkova P (2015). Reprogramming of cell fate: epigenetic memory and the erasure of memories past. EMBO J 34, 1296–1308.
Olsson A, Venkatasubramanian M, Chaudhri VK, Aronow BJ, Salomonis N, Singh H, Grimes HL (2016). Single-cell analysis of mixed-lineage states leading to a binary cell fate choice. Nature 537, 698–702.
Ozbudak EM, Thattai M, Lim HN, Shraiman BI, van Oudenaarden A (2004). Multistability in the lactose utilization network of Escherichia coli. Nature 427, 737–740.
Pedicini M, Barrenäs F, Clancy T, Castiglione F, Hovig E, Kanduri K, Santoni D, Benson M (2010). Combining network modeling and gene expression microarray analysis to explore the dynamics of Th1 and Th2 cell regulation. PLoS Comput Biol 6, e1001032.
Peine M, Rausch S, Helmstetter C, Fröhlich A, Hegazy AN, Kühl AA, Grevelding CG, Höfer T, Hartmann S, Löhning M (2013). Stable T-bet+GATA-3+ Th1/Th2 hybrid cells arise in vivo, can develop directly from naive precursors, and limit immunopathologic inflammation. PLoS Biol 11, e1001633.
Pillai M, Jolly MK (2021). Systems-level network modeling deciphers the master regulators of phenotypic plasticity and heterogeneity in melanoma. IScience 24, 103111.
Puniya BL, Todd RG, Mohammed A, Brown DM, Barberis M, Helikar T (2018). A mechanistic computational model reveals that plasticity of CD4+ T cell differentiation is a function of cytokine composition and dosage. Front Physiol 9, 878.
Radens CB, Blake D, Jewell P, Barash Y, Lynch KW (2021). Meta-analysis of transcriptomic variation in T cell populations reveals novel signatures of gene expression and splicing. RNA 26, 1320–1333.
Radens CM, Blake D, Jewell P, Barash Y, Lynch KW (2020). Meta-analysis of transcriptomic variation in T-cell populations reveals both variable and consistent signatures of gene expression and splicing. RNA 26, 1320–1333.

Renaude E, Kroemer M, Borg C, Peixoto P, Hervouet E, Loyon R, Adotévi O (2021). Epigenetic reprogramming of CD4+ helper T cells as a strategy to improve anticancer immunotherapy. Front Immunol 12, 669992.
Sanders VM (2006). Epigenetic regulation of Th1 and Th2 cell development. Brain Behav Immun 20, 317–324.
Santillan M (2008). On the use of the hill functions in mathematical models of gene regulatory networks. Math Model Nat Phenom 3, 85–97.
Santos-Moreno J, Tasiudi E, Stelling J, Schaerli Y (2020). Multistable and dynamic CRISPRi-based synthetic circuits. Nat Comm 11, 2746.
Sarkar S, Sinha SK, Levine H, Jolly MK, Dutta PS (2019). Anticipating critical transitions in epithelial-hybrid-mesenchymal cell-fate determination. Proc Natl Acad Sci USA 116, 26343–26352.
Sasaki T, Onodera A, Hosokawa H, Watanabe Y, Horiuchi S, Yamashita J, Tanaka H, Ogawa Y, Suzuki Y, Nakayama T (2013). Genome-wide gene expression profiling revealed a critical role for GATA3 in the maintenance of the th2 cell identity. PLoS One 8, e66468.
Serresi M, Kertalli S, Li L, Schmitt MJ, Dramaretska Y, Wierikx J, Hulsman D, Gargiulo G (2021). Functional antagonism of chromatin modulators regulates epithelial-mesenchymal transition. Sci Adv 7, eabd7974.
Somarelli JA, Shetler S, Jolly MK, Wang X, Bartholf Dewitt S, Hish AJ, Gilja S, Eward WC, Ware KE, Levine H, *et al*. (2016). Mesenchymal-epithelial transition in sarcomas is controlled by the combinatorial expression of MicroRNA 200s and GRHL2. Mol Cell Biol 36, 2503–2513.
Stadhouders R, Lubberts E, Hendriks RW (2018). A cellular and molecular view of T helper 17 cell plasticity in autoimmunity. J Autoimmun 87, 1–15.
Stark JM, Tibbitt CA, Coquet JM (2019). The metabolic requirements of Th2 cell differentiation. Front Immunol 10, 2318.
Subramanian A, Tamayo P, Mootha VK, Mukherjee S, Ebert BL, Gillette MA, Paulovich A, Pomeroy SL, Golub TR, Lander ES, *et al*. (2005). Gene set enrichment analysis: A knowledge-based approach for interpreting genome-wide expression profiles. Proc Natl Acad Sci USA 102, 15545–15550.
Suelves M, Carrio E, Nunez-Alvarez Y, Peinado MA (2016). DNA methylation dynamics in cellular commitment and differentiation. Brief Funct Genomics 15, 443–453.
Tkacik G, Walczak AM, Bialek W (2009). Optimizing information flow in small genetic networks. Phys Rev E Stat Nonlin Soft Matter Phys 80, 031920.
Tortola L, Jacobs A, Pohlmeier L, Obermair FJ, Ampenberger F, Bodenmiller B, Kopf M (2020). High-dimensional T helper cell profiling reveals a broad diversity of stably committed effector states and uncovers interlineage relationships. Immunity 53, 597–613.e6.
Touzot M, Grandclaudon M, Cappuccio A, Satoh T, Martinez-Cingolani C, Servant N, Manel N, Soumelis V (2014). Combinatorial flexibility of cytokine function during human T helper cell differentiation. Nat Commun 5, 3987.
Tripathi S, Levine H, Jolly MK (2020). The physics of cellular decision-making during epithelial-mesenchymal transition. Annu Rev Biophys 49, 1–18.
Wei G, Wei L, Zhu J, Zang C, Hu-Li J, Yao Z, Cui K, Kanno Y, Roh TY, Watford WT, *et al*. (2009). Global Mapping of H3K4me3 and H3K27me3 reveals specificity and plasticity in lineage fate determination of differentiating CD4+ T cells. Immunity 30, 155–167.
Wei L, Vahedi G, Sun HW, Watford WT, Takatori H, Ramos HL, Takahashi H, Liang J, Gutierrez-Cruz G, Zang C, *et al*. (2010). Discrete roles of STAT4 and STAT6 transcription factors in tuning epigenetic modifications and transcription during T helper cell differentiation. Immunity 32, 840–851.
Wilson CB, Rowell E, Sekimata M (2009). Epigenetic control of T-helper-cell differentiation. Nat Rev Immunol 9, 91–105.
Xhangholi I, Dura B, Lee G, Kim D, Xiao Y, Fan R (2019). Single-cell analysis of CAR-T cell activation reveals a mixed TH1/TH2 response independent of differentiation. Genomics Proteomics Bioinformatics 17, 129–139.
Yang P, Qian F-Y, Zhang M-F, Xu A-L, Wang X, Jiang B-P, Zhou L-L (2019). Th17 cell pathogenicity and plasticity in rheumatoid arthritis. J Leukoc Biol 106, 1233–1240.
Zhao W, Qiao L, Yan S, Nie Q, Zhang L (2021). Mathematical modeling of histone modifications reveals the formation mechanism and function of bivalent chromatin. IScience 24, 102732.
Zhou JX, Huang S (2011). Understanding gene circuits at cell-fate branch points for rational cell reprogramming. Trends Genet 27, 55–62.
Zhou L, Chong MMW, Littman DR (2009). Plasticity of CD4+ T cell lineage differentiation. Immunity 30, 646–655.
Zhu J, Jankovic D, Oler AJ, Wei G, Sharma S, Hu G, Guo L, Yagi R, Yamane H, Punkosdy G, *et al*. (2012). The transcription factor T-bet is induced by multiple pathways and prevents an endogenous Th2 cell program during Th1 cell responses. Immunity 37, 660–673.
Zhu R, del Rio-Salgado JM, Garcia-Ojalvo J, Elowitz MB (2022). Synthetic multistability in mammalian cells. Science 375, eabg9765.